

## Quantum size effect on Shubnikov-de Haas oscillations in 100nm diameter singlecrystalline bismuth nanowire

Jeongmin Kim, Dohun Kim, Taehoo Chang, and Wooyoung Lee

Citation: Applied Physics Letters 105, 123107 (2014); doi: 10.1063/1.4896543

View online: http://dx.doi.org/10.1063/1.4896543

View Table of Contents: http://scitation.aip.org/content/aip/journal/apl/105/12?ver=pdfcov

Published by the AIP Publishing

## Articles you may be interested in

Magnetism, magnetoresistance, and Shubnikov-de Haas oscillations in Na-implanted highly oriented pyrolitic graphite

J. Appl. Phys. 111, 093922 (2012); 10.1063/1.4709731

Shubnikov-de Haas measurement of electron effective mass in GaAs1 x Bi x

Appl. Phys. Lett. 99, 162108 (2011); 10.1063/1.3655198

Shubnikov-de Haas oscillations in an individual single-crystalline bismuth nanowire grown by on-film formation of nanowires

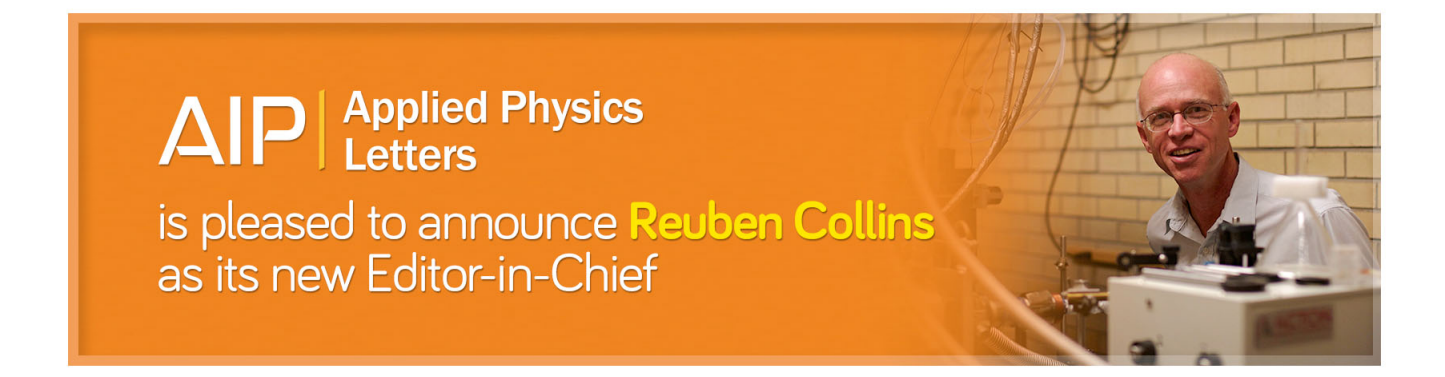
Appl. Phys. Lett. 95, 232107 (2009); 10.1063/1.3267143

Shubnikov-de Haas oscillations of the conductivity of a two-dimensional gas in quantum wells based on germanium and silicon. Determination of the effective mass and g factor

Low Temp. Phys. 35, 141 (2009); 10.1063/1.3075945

The Shubnikov-de Haas effect and high pressure

Low Temp. Phys. 27, 691 (2001); 10.1063/1.1401175





## Quantum size effect on Shubnikov-de Haas oscillations in 100 nm diameter single-crystalline bismuth nanowire

Jeongmin Kim, <sup>1,a)</sup> Dohun Kim, <sup>2,a)</sup> Taehoo Chang, <sup>1</sup> and Wooyoung Lee <sup>1,b)</sup> <sup>1</sup>Department of Materials Science and Engineering, Yonsei University, 134 Shinchon, Seoul 120-749, South Korea

<sup>2</sup>Department of Physics, University of Maryland, College Park, Maryland 20742, USA

(Received 7 April 2014; accepted 13 September 2014; published online 23 September 2014)

Quantum size effect (QSE) in Bi nanowire is theoretically predicted to decrease band overlap energy resulting in semimetal-to-semiconductor transition. However, this effect has been rarely demonstrated on transport properties because of carrier-surface scattering and charge carriers induced from surface states of Bi. We report QSE on Shubnikov-de Haas (SdH) oscillations in a single-crystalline Bi nanowire with a diameter of 100 nm. The variation of intrinsic properties estimated using SdH oscillations indicates that the subband energy shift due to QSE. The enhanced effective mass of the electrons is consistent with the theoretical prediction pertaining to strong electron-hole coupling of Bi. © 2014 AIP Publishing LLC. [http://dx.doi.org/10.1063/1.4896543]

Low-dimensional nanostructures are considered to be promising thermoelectric performance-enhancing materials due to quantum size effects (QSE). 1-17 In particular, one-dimensional nanowires based on bismuth (Bi) have been intensively investigated for the enhancement of thermoelectric performance based on semimetal-to-semiconductor (SMSC) transitions.<sup>3</sup> This phenomenon originates from the unusual physical properties of semimetal Bi such as long Fermi wavelength (~70 nm) and small effective mass  $(\sim 0.001 \, m_{\rm e})$  of charge carriers.<sup>3–5</sup> On the basis of carefully calculated band-edge energies in Bi nanowires, previous studies have reported that the subbands energy shift for the L-point electron pockets due to QSE begins to occur for diameters of approximately 400 nm,<sup>3</sup> and the band gap opening between the *L*- and *T*-point subbands (SMSC transition) leads to an increase in the thermoelectric figure of merit  $(ZT = S^2 \sigma T / \kappa$ , where S,  $\sigma$ , T, and  $\kappa$  are the Seebeck coefficient, electrical conductivity, temperature, and thermal conductivity, respectively) as the diameter decreases.<sup>3,4</sup> However, the reported thermoelectric properties of Bi nanowires, such as S and  $\sigma$ , have not exceeded the values for bulk Bi. 6-9 The small S and  $\sigma$  are attributable to a finite size effect of the nanowire structure; meanwhile, a decrease in the mean free path (MFP) of carriers is due to carrier-surface scattering. Moreover, the subband energy shift leads to an increase of the electron effective mass owing to strong coupling between the valence and conduction band of electron Fermi pockets of Bi.<sup>3,4,10</sup> This increase of effective mass causes the critical nanowire diameter, below which the SMSC transition occurs, to decrease from 50 nm to 30 nm.<sup>3,4</sup> To observe these effects experimentally, studies on the carrier transport properties of Bi nanowires were performed in array-type <sup>6,9,11–15</sup> and individual <sup>5,17–20</sup> nanowires. In these previous studies, magneto-transport experiments, including Shubnikov-de Haas (SdH), 9,14,15,18,19 Ahronov-Bohm (AB)

oscillations, <sup>16</sup> and universal conductance fluctuation (UCF),<sup>17</sup> could be useful tools to investigate the nanowire structures. SdH oscillations, in particular, are a powerful means for estimating the intrinsic properties of carriers near the Fermi level such as carrier density, mobility, and quasiparticle effective mass. 14,15,18,19,21,22 However, previous studies using SdH oscillations have failed to exhibit direct signatures of the subbands energy shift originated from QSE. First, a quantitative analysis for the array-type nanowire samples was difficult owing to random orientation of the nanowires with respect to the applied magnetic fields. Second, in the studies for an individual Bi nanowire, the diameter of the measured nanowires was not sufficient to observe the subbands energy shift. The SdH oscillations reported in 400 nm Bi nanowire showed that the periods of SdH are significantly similar to the values of bulk Bi, which reflects that the Bi nanowires have bulk-like properties above the diameter of 400 nm as reported in the theoretical prediction. 18,19 Other SdH experiment performed with small diameter Bi nanowire (<50 nm), the transport properties were reported to be dominated by the surface state of Bi when the nanowire diameter was reduced to 45 nm. <sup>16</sup> Despite the fact that the 45 nm nanowire diameter is close to the theoretically predicted critical diameter (~30 nm) for the SMSC transition, the change in the intrinsic transport properties of Bi nanowires has not been clearly demonstrated owing to the metallic surface states. 17 Therefore, the intermediate diameter region (50 < d < 200 nm) is preferred candidate for clearly studying the variation of intrinsic properties due to the subbands energy shift.

In this work, we studied the SdH oscillations in an individual single-crystalline Bi nanowire with a diameter of 100 nm in an effort to investigate changes of the intrinsic properties of a Bi nanowire with diameters of a certain range that cause the subbands energy shift without the surface states effect. The intrinsic properties such as effective mass and carrier density were estimated by analyzing the period and amplitude of the SdH. In particular, the estimated effective mass was found to be significantly larger than the value

<sup>&</sup>lt;sup>a)</sup>J. Kim and D. Kim contributed equally to this work.

b) Author to whom correspondence should be addressed. Electronic mail: wooyoung@yonsei.ac.kr

predicted by theoretical studies considering QSE and electron-hole coupling.<sup>3,4</sup> We also discuss the correlation between the increase in the effective mass and the Seebeck coefficient with decreasing diameter to interpret the reported small Seebeck coefficient of Bi nanowires.

We have investigated the intrinsic transport properties of single-crystalline Bi nanowires grown using the on-film formation of nanowires (OFF-ON) method. 20,23 The growth method and device fabrication process are described in detail elsewhere. 17-20 To summarize briefly, a 50-nm-thick Bi film was deposited on a thermally oxidized Si (100) substrate using a radio-frequency sputtering system at room temperature, with a deposition pressure of  $2 \times 10^{-3}$  Torr. The Bi thin film was annealed to grow nanowires at 250 °C for 5 h using a custom-made vacuum  $(10^{-7} \text{Torr})$  furnace. The single-crystalline Bi nanowires were spontaneously grown on the Bi thin film to release a stress induced by thermal expansion mismatch between the Bi thin film and silicon oxide layer.<sup>20</sup> The low-magnification transmission electron microscopy (TEM) image shows a Bi nanowire with a diameter of 100 nm, which was grown along the [100] direction of a hexagonal cell with an oxide layer of 10 nm thickness (Fig. 1(a)). The rhombohedral structure of Bi can be defined as a Cartesian coordinate system with binary, bisectrix, and trigonal axes. <sup>13</sup> As shown in Fig. 1(b), the direction of [100] in a hexagonal cell coincides with the binary axis in the reciprocal lattice, and is perpendicular to the orientations of a single hole and one-electron Fermi surface pockets, which are trigonal axis and  $6.5^{\circ}$  tilted from the bisectrix axis, respectively. A high-resolution TEM was used to analyze the crystalline structure of the Bi nanowire (Fig. 1(c)). The TEM sample was prepared by slicing the wire normal to the growth direction using a focused ion beam (FIB). The separation of the lattice fringes of the Bi nanowire (3.96 Å) are consistent with a lattice plane spacing of the (003) plane with a lattice constant of 11.88 Å, which is approximately equal to that of a bulk Bi crystal  $(c = 11.862 \text{ Å}; \text{ JCPDS card no. } 85-1329).^{25}$  The corresponding selected-area electron diffraction (SAED) pattern obtained on the [100] zone axis confirmed that the Bi nanowire is a high-quality single-crystal with growth direction along [100] (Fig. 1(d)).

To fabricate an individual nanowire device for the magnetoresistance (MR) measurements, the Bi nanowires were dispersed by direct contact of as-grown nanowires substrate on a thermally oxidized Si substrate. Four-terminal electrodes were defined using electron-beam lithography and Cr (5 nm)/Au (150 nm) metallization was performed using a DC sputtering system. To obtain ohmic contact between the Bi nanowire and the electrodes, an inductively coupled Ar plasma etching technique was employed. 17-20 All measurements were performed using a commercial cryostat equipped with a 9T superconducting magnet (PPMS, Quantum Design, USA) with variations in temperature and magnetic field ranging from 1.8 to 12.4 K and 0 to 9 T, respectively. Figure 1(e) shows the nanowire device used for the MR measurement based on the 100-nm-diameter Bi nanowire and two different magnetic field geometries: Transverse and longitudinal. Since the Bi nanowire grew along the [100] direction, the magnetic field can be aligned precisely

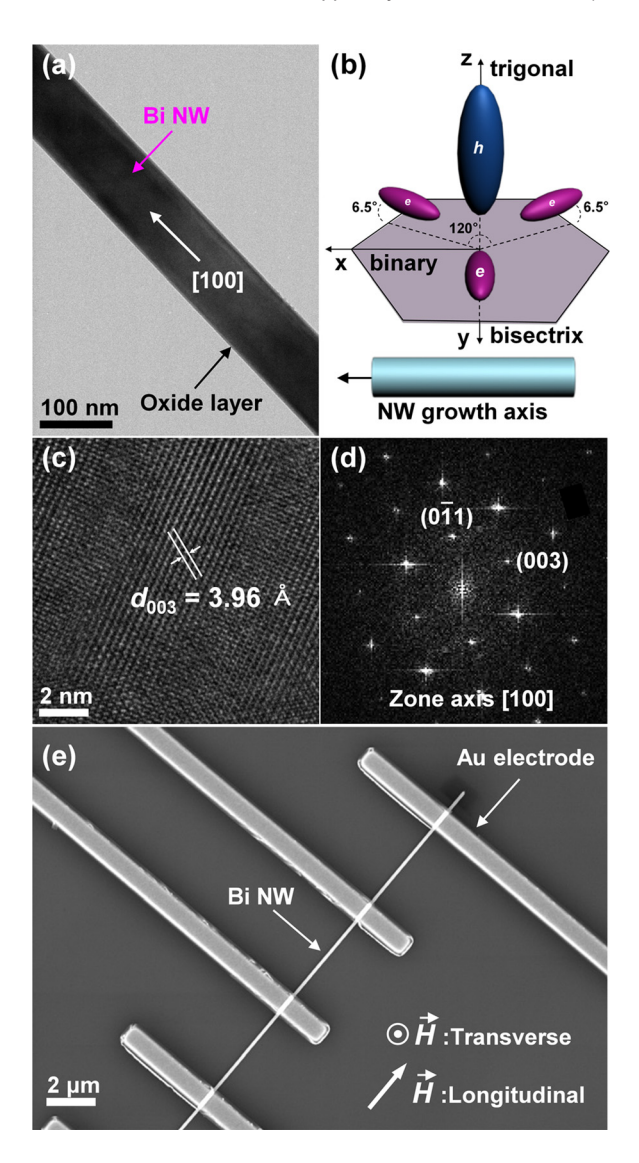


FIG. 1. (a) A low-magnification TEM image of a 100-nm-diameter Bi nanowire grown along the [100] direction. (b) Schematic of the three-electron and single-hole Fermi surface pockets of Bi. (c) A high-resolution TEM image obtained in the sliced Bi nanowire normal to the growth direction using a FIB. (d) An electron diffraction (ED) pattern of the sliced Bi nanowire with the [100] zone axis. (e) A scanning electron microscope (SEM) image of the four-terminal device with a 100 nm Bi nanowire.

with the binary axis in the longitudinal geometry. In the transverse geometry, however, we expect a larger uncertainty in the alignment between the magnetic field and a specific crystallographic axis due to the orientation mismatch induced during the nanowire dispersion process.

Figure 2 shows the MR of the device measured with magnetic fields ranging from 0 to 9 T in two different geometries: (a) transverse and (b) longitudinal. The transverse MR monotonically increases up to 300% with increasing magnetic field at 1.8 K (Fig. 2(a)). The overall MR with respect to magnetic field follows that of typical nonmagnetic metals, where the MR is positive and proportional to the cyclotron orbit  $\omega_c \tau$ , ( $\omega_c$  and  $\tau$  are the cyclotron frequency and relaxation time, respectively). The MR is roughly temperature-independent from 1.8 to 12.4 K, indicating that the MFP approaches the impurity-limited value.

For the longitudinal geometry, the measured MR exhibits a non-monotonic behavior as the magnetic field increases,

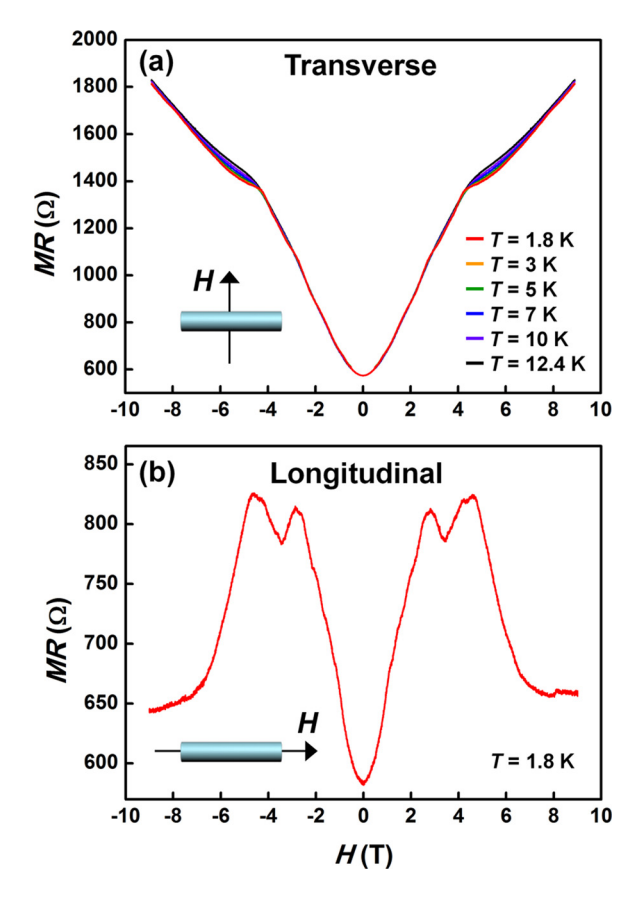


FIG. 2. MR of the 100-nm-diameter Bi nanowire in (a) the transverse geometry at  $T=1.8,\,3,\,5,\,7,\,10$ , and 12.4 K and (b) the longitudinal geometry at T=1.8 K. The insets of (a) and (b) show the orientation of the applied magnetic fields with nanowire direction for the transverse and longitudinal geometries.

as shown in Fig. 2(b). This behavior can be explained by a quasi-classical effect involving the surface wall scattering that occurs when the magnetic field is smaller than the Chambers magnetic field,  $H_c = \Phi_0 k_F / \pi d$ , where  $\Phi_0 = hc/e$  (h is Planck's constant) and  $k_F$  and d are the Fermi wave vector and wire diameter, respectively. 14,15 The orbit diameter of the Landau level is the same as the nanowire diameter at  $H = H_c$ . When  $H < H_c$ , the large Landau level orbit diameter causes an increase in MR due to surface scattering. Conversely, the MR decreases in the case of  $H > H_c$  owing to the reduction of surface scattering, and ballistic transport of carriers in the direction of magnetic fields parallel with the transport direction in the longitudinal geometry. For the 100-nm-diameter Bi nanowire,  $H_c$  was found to be  $\sim$ 2 T, which is less than the observed crossover field of  $\sim$ 3 T but is in good agreement with the diameter dependency of  $H_c$ when taking into account the 10-nm-thick oxide layer. 14,15,19 Therefore, we expect that SdH oscillations can be observed when a magnetic field larger than  $H_c$  is applied in the longitudinal configuration.

Figure 3 shows the SdH oscillations of the 100-nm-diameter Bi nanowire in the transverse (a) and longitudinal (b) geometries, which was obtained by subtracting the MR data at 12.4 K, i.e., MR(T) - MR(T = 12.4 K). The SdH oscillations have a periodicity related to the Fermi surface pocket in the inverse magnetic fields, where the period is given by<sup>27</sup>

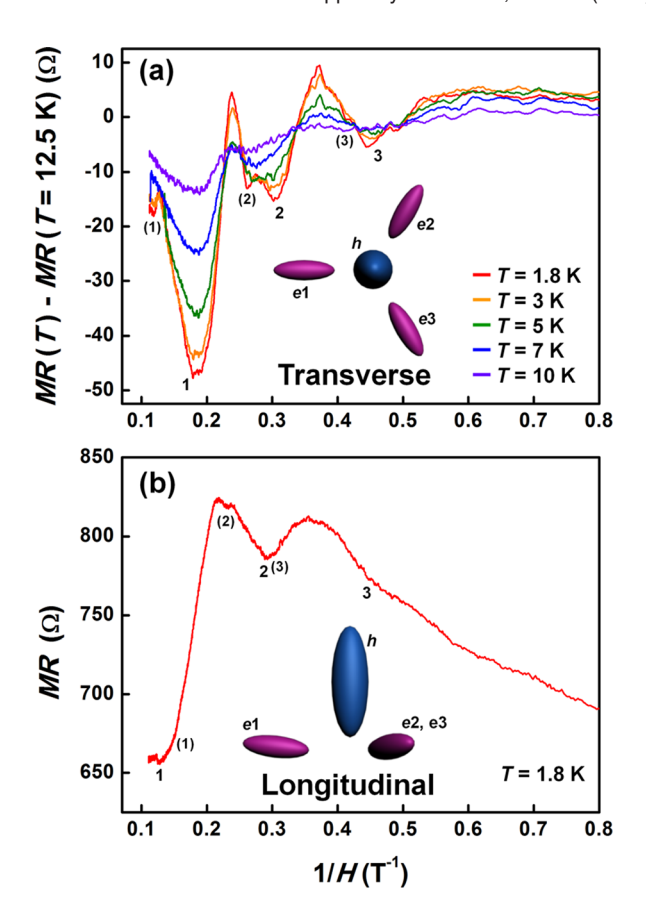


FIG. 3. SdH oscillations of the 100-nm-diameter Bi nanowire as a function of inverse magnetic field 1/H, displayed as (a)  $MR(T) - MR(T = 12.4 \,\mathrm{K})$  in the transverse geometry and (b)  $MR(T = 1.8 \,\mathrm{K})$  in the longitudinal geometry. The indicators, n and (n), represent the origin of each SdH peak, electron and hole, respectively. The insets show schematics of the Fermi surface pockets along the orientation of magnetic field.

$$\Delta \left(\frac{1}{H}\right) = \frac{2\pi}{\hbar cA} \,, \tag{1}$$

where A is the cross sectional area of the Fermi surface pocket perpendicular to the magnetic field. When there are several Fermi surface pockets in the Brillouin zone, as for Bi, each period is overlapped in SdH oscillations. In the transverse geometry, the two different oscillations were found to be 0.144 ( $\pm 0.02$ ) and 0.148 ( $\pm 0.006$ ) T<sup>-1</sup> of the period. Note that although the error range of 0.144 period is significantly large compared to the difference between the two periods, it is possible to distinguish them by their different amplitudes. For example, because the mobility of electrons is larger than that of holes in Bi, the period which has larger amplitude (0.144 T<sup>-1</sup>), must originate from electron pockets.<sup>27</sup> The large error size of the electron period is due to the moment of the Fermi level, which leads to a reduction in the period for high magnetic fields. 27,28 Owing to the symmetry of electron pockets in the transverse configuration, as shown in the inset of Fig. 3(a), the periods for the hole and electron pockets are estimated to be  $\Delta(1/H)_{T,e1}$  $\approx \Delta(1/H)_{T,e^2} \approx \Delta(1/H)_{T,e^3} \approx 0.144 \,\mathrm{T}^{-1}$  and  $\Delta(1/H)_{T,h} \approx 0.148 \,\mathrm{T}^{-1}$ . The period of electron (hole) pockets is slightly larger (smaller) than the minimum (maximum) period of  $0.135\,\mathrm{T}^{-1}\,(0.16\,\mathrm{T}^{-1})^{27,29}$  because the alignment of the magnetic field to a specific crystallographic orientation is difficult to achieve for the nanowire structure. Conversely, the

longitudinal magnetic field can easily be aligned with the binary axis using the long axis of the nanowire. In the longitudinal geometry, there are three different cross sections  $(A_h,$  $A_{e1}$ , and  $A_{e2} = A_{e3}$ ) of Fermi surface pockets, as illustrated in the inset of Fig. 3(b). However, two different periods for the SdH oscillations have been extracted, since the cross sections of e2 and e3 pockets are too small to contribute to SdH oscillations in the 100-nm-diameter nanowire. The period of the smallest pocket along the binary axis is larger than  $0.8\,\mathrm{T}^{-1}$ , which is over  $1/H_c = 0.5 \,\mathrm{T}^{-1}$ . Therefore, the periods of the e1 and h pockets are found to be  $\Delta(1/H)_{L,e1} \approx 0.159$  $(\pm 0.006) \text{ T}^{-1}$  and  $\Delta(1/H)_{L,h} \approx 0.075 \ (\pm 0.001) \text{ T}^{-1}$ , respectively, which are in good agreement with that of a 400-nmdiameter Bi nanowire  $(0.16 \text{ and } 0.074 \text{ T}^{-1})^{19}$  and a Bi thin film  $(0.17 \text{ and } 0.08 \text{ T}^{-1})$ . This indicates accurate alignment of the longitudinal magnetic fields with the long axis of the Bi nanowire grown along the binary axis. Table I represents the magnetic field of the SdH minima and its origin. We estimate the carrier concentrations using the period of the SdH oscillations, which is given by 18,30

$$n = \frac{1}{3\pi^2} \left(\frac{2e}{\hbar}\right)^{3/2} \left(\frac{1}{\Delta(1/H)_{\perp} \Delta(1/H)_{\perp} \Delta(1/H)_{\parallel}}\right)^{-1/2}, \quad (2)$$

where  $\Delta(1/H)_{\perp}$  and  $\Delta(1/H)_{\parallel}$  are the periods of the SdH oscillation for magnetic fields perpendicular and parallel to the major axis of the Fermi pocket, respectively. For the parallel magnetic fields of the electron pocket, the cross sectional area,  $A_{\parallel}$  is too small to obtain  $\Delta(1/H)_{\parallel}$ .<sup>27</sup> As a result, the concentration of electrons can be expected to be smaller than the estimated value  $2.81 \times 10^{17} \, \mathrm{cm}^{-3}$ , which is calculated using  $\Delta(1/H)_{T,e}$  and  $\Delta(1/H)_{L,e}$ . In the case of holes,  $\Delta(1/H)_{\perp}$  and  $\Delta(1/H)_{\parallel}$  are considered to be  $\Delta(1/H)_{L,h}$  and  $\Delta(1/H)_{T,h}$ , respectively. The concentration of holes was found to be  $1.96 \times 10^{17} \, \mathrm{cm}^{-3}$ . The estimated concentrations of electrons and holes are small compared to the carrier concentration of bulk Bi,  $n=p=3.7 \times 10^{17} \, \mathrm{cm}^{-3}$ .<sup>26</sup>

Furthermore, using the temperature dependence of the SdH oscillation amplitude, we are able to extract the cyclotron effective mass of carriers,  $m_c^{*.13}$  The amplitudes, AMP (T) of the SdH oscillations are plotted as the ratio of that at two different temperatures and fitted by<sup>21,22</sup>

$$\frac{AMP(H,T_1)}{AMP(H,T_2)} = \frac{T_1 \sinh\left[\frac{2\pi^2 k_B T_2 m_c^*}{\hbar e H}\right]}{T_2 \sinh\left[\frac{2\pi^2 k_B T_1 m_c^*}{\hbar e H}\right]},$$
(3)

TABLE I. SdH oscillation minima of the Bi nanowire, in 1/H ( $T^{-1}$ ), and the origin of SdH in the transverse and longitudinal geometries.

Transverse		Longitudinal	
$1/H (T^{-1})$	Origin (n)	$1/H(T^{-1})$	Origin (n)
0.179	e1(1), e2(1), e3(1)	0.129	e1(1)
0.307	<i>e</i> 1(2), <i>e</i> 2(2), <i>e</i> 3(2)	0.292	e1(2)
0.466	<i>e</i> 1(3), <i>e</i> 2(3), <i>e</i> 3(3)	0.447	e1(3)
0.118	h(1)	0.155	h(1)
0.261	h(2)	0.229	h(2)
0.413	h(3)	0.305	h(3)

using  $m_c^*$  as a fitting parameter. Figure 4 shows the fitted results for the ratio of the amplitudes, AMP(1.8 K)/AMP(10 K) and AMP(3 K)/AMP(10 K) using electron SdH oscillations in the transverse geometry. To compare the estimated cyclotron effective mass of the Bi nanowire, we calculated the cyclotron effective mass of bulk Bi using the effective mass tensor<sup>3</sup>

$$m_c^* = \left(\frac{\det \mathbf{M}_e}{\hat{\mathbf{I}} \mathbf{M}_e \hat{\mathbf{I}}}\right)^{1/2}.$$
 (4)

Here,  $\mathbf{M}_e$  is the electron effective mass tensor and  $\hat{\mathbf{I}}$  is the unit vector along the nanowire direction. The cyclotron effective mass of the electron calculated using Eq. (4) in the binary axis of bulk Bi is  $0.0118 m_0$ . However, the calculated value is an approximation of three electron Fermi pockets in the binary axis. Since the cyclotron effective masses of the three pockets can vary depending on the direction of the magnetic fields, we should take into account the effective mass tensors of the three different pockets. In the nanowire grown along the binary axis, the effective mass of the e1 pocket is 0.0012  $m_0$ , 0.2959  $m_0$ , and 0.0023  $m_0$  in the direction of the binary-, bisectrix-, and trigonal axis, respectively.<sup>3</sup> The effective masses of e2 and e3 are the same:  $0.1975 \ m_0$ ,  $0.0016 \ m_0$ , and  $0.0023 \ m_0$  in the each direction.<sup>3</sup> The cyclotron effective masses calculated using Eq. (4) are  $0.0179 m_0$  for the e1 pocket and  $0.0178 m_0$  for the e2 and e3 pockets. By comparing these values to the estimated cyclotron effective mass  $(0.0624 m_0)$  using the amplitude of the SdH oscillations, we found that the effective mass for electrons in the 100-nm-diameter Bi nanowire is three times larger than that of bulk Bi.

Note that for accurate comparison, the concentration and effective mass estimated from a large diameter nanowire with bulk characteristics are needed. Although the bulk properties of Bi nanowires with a diameter of 400 nm were confirmed by SdH oscillation, the preferred crystallographic orientation for a large diameter nanowire was found to be different to that for Bi nanowires with a diameter of 100 nm. <sup>18,19</sup> Therefore, the reported values for bulk Bi with

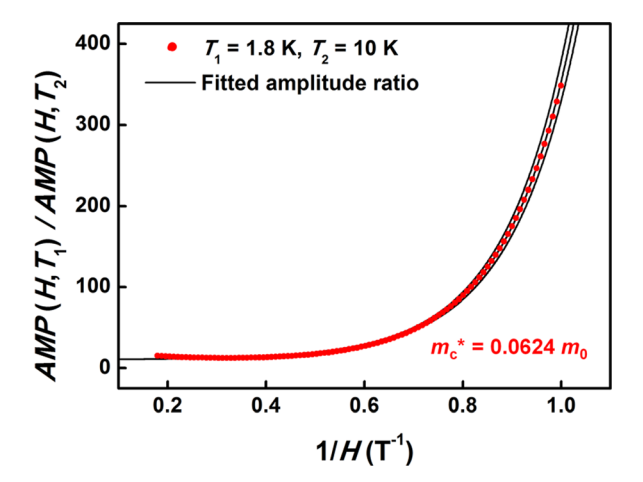


FIG. 4. SdH oscillation amplitudes at 1.8 K (red points), displayed as ratios to the same measurement at 10 K. The solid line is the fitted amplitude ratio obtained using Eq. (3). The evaluated cyclotron effective mass from the fitted line is  $m_c^* = (0.0624 \pm 4.2 \times 10^{-5}) \ m_0$ . The upper  $(m_c^* = 0.0630 \ m_0)$  and lower  $(m_c^* = 0.0618 \ m_0)$  solid lines show the precision of the fitting.

various crystallographic geometries and under varying magnetic fields were used instead.

The Lax two-band model used in previous theoretical studies showed that the subband energy shifting for L-point electron pockets leads to an increase of electron effective mass owing to strong coupling between the conduction and valence bands, where the effective mass is given by the following relationship:<sup>4,10</sup>

$$\frac{1}{m^*} = \frac{1}{m_0} + \frac{2}{m_0^2} \frac{|\langle v|p|c\rangle|^2}{E_g} - \frac{12\hbar^2 k^2 |\langle v|p|c\rangle|^4}{E_g^3 m_0^2}.$$
 (5)

In this equation,  $|\langle v|p|c\rangle|$  and  $E_g$  are, respectively, coupling strength and energy gap between the valence v and conduction band c. At the band edge (k = 0), electron effective mass increases with the band gap at constant coupling strength. 10 From Eq. (5) and the calculated band edge energy, the cyclotron effective mass was calculated as two times larger (0.04  $m_0$ ) than for bulk Bi, which is smaller than the estimated cyclotron effective mass using SdH. An increase of the effective mass not only decreases the critical diameter of the SMSC transition but also affects the Seebeck coefficient. The two-band model<sup>3,4</sup> can be used to determine the Seebeck coefficient and electrical conductivity in semimetal thermoelectric materials such as Bi. The total Seebeck coefficient ( $S_{\text{total}}$ ) is determined by the partial conductivity ( $\sigma_n$ ) and partial Seebeck coefficient  $(S_n)$  of the electron and hole bands as  $S_{\text{total}} = (\sigma_e S_e + \sigma_h S_h)/(\sigma_e + \sigma_h)$  for Bi, where n is e or h for the electron or hole bands, respectively.  $S_{\rm total}$  is highly sensitive to  $\sigma_n$  owing to the opposite signs of  $S_e$  and  $S_h$ . Since the value of  $S_{\text{total}}$  for typical Bi is a negative value, the contribution of  $S_e$  decreases with the weighting factor  $\sigma_e$ , resulting in an overall reduction of  $S_{\text{total}}$ . Therefore, our observations which show that a decrease in the concentration and an increase in the effective mass of electrons for the Bi nanowire with  $d = 100 \,\mathrm{nm}$  can explain the decrease in the Seebeck coefficient for Bi nanowires. 6-9 Furthermore, in the small diameter Bi nanowire, the finite size effect such as carrier-surface scattering also causes the decrease of the Seebeck coefficient.9

In summary, quantum size effect on the SdH oscillations in an individual single-crystalline Bi nanowire with a diameter of 100 nm grown using the OFF–ON method were investigated. From the measured periods of SdH oscillations in the transverse and longitudinal geometries, we found that the intrinsic electron and hole concentrations at the Fermi level are less than those of bulk Bi. This finding can be attributed to quantum confinement induced subbands energy shift. From the amplitudes of the SdH oscillations, we also observed that the effective mass of electrons is three times larger in the Bi nanowire than that of bulk Bi. Our findings are the first to demonstrate the changes in intrinsic properties due to subbands energy shift originated from QSE and

electron-hole coupling in Bi nanowire, and offer an explanation for the smaller Seebeck coefficients observed in Bi nanowires compared to those in bulk Bi.

This work was supported by the Priority Research Centers Program (No. 2009-0093823) and the Pioneer Research Center Program (No. 2013008070) through the National Research Foundation of Korea (NRF).

L. D. Hicks and M. S. Dresselhaus, Phys. Rev. B 47, 12727–12731 (1993).
 L. D. Hicks and M. S. Dresselhaus, Phys. Rev. B 47, 16631–16634 (1993).
 Y. Lin, X. Sun, and M. S. Dresselhaus, Phys. Rev. B 62, 4610–4623 (2000).

<sup>4</sup>T. W. Cornelius and M. E. T. Molares, *Nanowires*, edited by P. Prete (InTech, Rijeka, 2010), Vol. 14.

<sup>5</sup>S. Lee, J. Ham, K. Jeon, J. Noh, and W. Lee, Nanotechnology **21**, 405701 (2011)

<sup>6</sup>J. Heremans and C. M. Thrush, Phys. Rev. B **59**, 12579–12583 (1999).

<sup>7</sup>Y. Lin, O. Rabin, S. B. Cronin, J. Ying, and M. S. Dresselhaus, Appl. Phys. Lett. **81**, 2403–2405 (2002).

<sup>8</sup>A. Nikolaeva, T. E. Huber, D. Gitsu, and L. Konopko, Phys. Rev. B 77, 035422 (2008).

<sup>9</sup>T. E. Huber, A. Adeyeye, A. Nikolaeva, L. Konopko, R. C. Johnson, and M. J. Graf, Phys. Rev. B 83, 235414 (2011).

<sup>10</sup>M. R. Black, Y. Lin, S. B. Cronin, O. Rabin, and M. S. Dresselhaus, Phys. Rev. B 65, 195417 (2002).

<sup>11</sup>Z. Zhang, X. Sun, M. S. Dresselhaus, J. Y. Ying, and J. Heremans, Phys. Rev. B 61, 4850–4861 (2000).

<sup>12</sup>Z. Zhang, X. Sun, M. S. Dresselhaus, J. Y. Ying, and J. P. Heremans, Appl. Phys. Lett. **73**, 1589–1591 (1998).

<sup>13</sup>J. Heremans, C. M. Thrush, Y. M. Lin, S. Cronin, Z. Zhang, M. S. Dresselhaus, and J. F. Mansfield, Phys. Rev. B 61, 2921–2930 (2000).

<sup>14</sup>T. E. Huber, A. Nikolaeva, D. Gitsu, L. Konopko, C. A. Foss, Jr., and M. J. Graf, Appl. Phys. Lett. 84, 1326–1328 (2004).

<sup>15</sup>T. E. Huber, A. Nikolaeva, L. Konopko, and M. J. Graf, Phys. Rev. B 79, 201304(R) (2009).

<sup>16</sup>L. Konopko, T. Huber, and A. Nikolaeva, J. Low Temp. Phys. 159, 253–257 (2010).

<sup>17</sup>J. Kim, S. Lee, Y. M. Brovman, M. Kim, P. Kim, and W. Lee, Appl. Phys. Lett. **104**, 043105 (2014).

<sup>18</sup>K. Lee, S. Lee, S. N. Holmes, J. Ham, W. Lee, and C. H. W. Barnes, Phys. Rev. B 82, 245310 (2010).

<sup>19</sup>W. Shim, J. Ham, J. Kim, and W. Lee, Appl. Phys. Lett. 95, 232107 (2009)

<sup>20</sup>W. Shim, J. Ham, K. Lee, W. Jeung, M. Johnson, and W. Lee, Nano Lett. 9, 18–22 (2009).

<sup>21</sup>B. Fluegel, R. N. Kini, A. J. Ptak, D. Beaton, K. Alberi, and A.

Mascarenhas, Appl. Phys. Lett. **99**, 162108 (2011). <sup>22</sup>W. Lange, F. A. P. Blom, and J. H. Wolter, Semicond. Sci. Technol. **8**,

341–343 (1993).
<sup>23</sup>J. Ham, W. Shim, D. H. Kim, S. Lee, J. Roh, S. W. Sohn, K. H. Oh, P. W.

Voorhees, and W. Lee, Nano Lett. 9, 2867–2872 (2009).

<sup>24</sup>R. D. Brown, R. L. Hartman, and S. H. Koenig, Phys. Rev. 172, 598–602 (1968).

<sup>25</sup>D. Schiferl and C. S. Barrett, J. Appl. Crystallogr. 2, 30–36 (1969).

<sup>26</sup>F. Y. Yang, K. Liu, K. Hong, D. H. Reich, P. C. Searson, and C. L. Chien, Science 284, 1335–1337 (1999).

<sup>27</sup>F. Y. Yang, K. Liu, K. Hong, D. H. Reich, P. C. Searson, C. L. Chien, Y. L. Wang, K. Y. Zhang, and K. Han, Phys. Rev. B 61, 6631–6636 (2000).

<sup>28</sup>G. E. Smith, G. A. Baraff, and J. M. Rowell, Phys. Rev. 135, A1118 (1964).

<sup>29</sup>J. S. Dhillon and D. Shoenberg, Philos. Trans. R. Soc. London A **248**, 1–21 (1955)

<sup>30</sup>R. N. Bhargava, Phys. Rev. **156**, 785–797 (1967).